A comprehensive approach for designing different configurations of isothermal reactors with fast catalyst deactivation

Tomás Cordero-Lanzac*, Andrés T. Aguayo, Ana G. Gayubo, Pedro Castaño, Javier Bilbao

Department of Chemical Engineering, University of the Basque Country (UPV/EHU), PO Box 644, 48080, Bilbao, Spain

Corresponding author: tomas.cordero@ehu.eus

ABSTRACT

A methodology for simulating the performance of different reactor configurations for processes with complex reaction networks and fast catalyst deactivation has been proposed. These reaction configurations are: packed bed, moving bed and fluidized bed reactors with and without catalyst circulation. From kinetic parameters collected in a packed bed reactor and a rigorous consideration of the activity, modifications in the convection-dispersion-reaction equation have led to the prediction of the catalyst performance in each reactor configuration. Circulating fluidized bed reactor has been simulated with an original model of parallel compartments, which allows for determining its performance in the steady state from the evolution of the transitory period. The methodology has been used for simulating the dynamics of SAPO-34 fast deactivation during the methanol-to-olefins (MTO) process. For each reactor configuration, concentration profiles and their evolution with time have been simulated, thus predicting the effect of reaction conditions and water content (formed and/or co-fed) on the activity profile or the activity distribution function (in the case of circulating fluidized bed reactor). The olefin yield and distribution have also been compared for each reactor configuration.

Keywords: Reactor design; deactivation; MTO, packed bed; circulating fluidized bed

1. Introduction

Catalytic processes are involved in the production of the majority of goods, consumables and commodities we use every day: fuels, chemicals and plastics, among others. Besides, novel catalysts are thrusting new processes for incorporating renewable and waste as raw materials. Within this framework, chemical industry is increasingly relying on new catalytic processes, materials and reactors to meet the changing market while satisfying environmental and safety issues. These catalysts cannot avoid some degree of deactivation, which is caused by coking, poisoning, degradation or attrition [1]. Among these causes, the deposition of coke has caught especial attention because it is inevitable in reactions involving organic compounds [2,3]. Moreover, it frequently causes a fast deactivation that finally determines the reactor configuration and the reaction-regeneration strategy. In these cases, the circulation of the catalyst is required, entering into play fluidized bed or moving bed reactors. Implemented and scaled-up examples of these reactors are the ones used in the fluidized catalytic cracking (FCC, a riser reactor) [4] or the methanol-to-olefins (MTO, a fluidized bed reactor) [5] processes; each of them with catalyst circulation for regeneration.

Reactor design for processes with fast deactivation and catalyst circulation has not received much attention within the literature. The pioneering and groundbreaking works of Levenspiel [6] and Kunii and Levenspiel [7] described the conceptual problem of fluidized bed reactors with catalyst circulation. However, they provided analytical solutions for the design equations in the case of simple reaction networks (one step) and deactivation kinetics independent on the reaction medium composition. Likewise, Fogler [8] reported the analytical solution of moving bed reactor design using the same type of deactivation kinetics. Nevertheless, most of the industrial catalyst processes involving organic compounds present complex reaction networks and the catalyst

deactivation is strongly influenced by the composition of the reaction medium. In this situation, analytical solutions cannot be provided because of the complexity of the given design equations.

A paradigmatic case study within these processes with complex reaction schemes and fast deactivation is the MTO, which offers a sustainable way (using natural gas, biomass or waste via gasification) for producing light olefins [9,10]. At industrial scale, MTO process commonly uses SAPO-34 catalysts and a fluidized bed reactor-regenerator system [5]. The main drive within this field has been increasing the light olefin selectivity (preferentially of propylene) and attenuates the catalyst deactivation by coking [9,11]. Modifications on the two commercial catalysts in the transformation of methanol, SAPO-34 and ZSM-5 zeolite, are mainly focused on their crystal size, microporous structure and acidity [10,12–16]. Briefly, SAPO-34 offers higher selectivity of olefins but a faster deactivation due to its small channels, big cages and high acidity [17].

The MTO reactor design requires a deactivation kinetic model that faithfully describes the influence of the reaction conditions and the reaction medium. Besides, the deactivation pathways or just the kinetic parameters of the deactivation kinetic model depend on the catalyst features [18]. The computation of deactivation kinetics in processes with complex kinetic networks as MTO requires a great amount of experimental data and an accurate monitoring of the product distribution during the reaction. Nonetheless, the crucial aspect is the development of a methodology able to take the “past history” of the catalyst into account [19,20]. This way, the evolution of the activity profile with time and the performance of the catalyst in reactor configurations in which experimental data are not collected could be estimated. A simultaneous modeling of the kinetics of all the steps of a complex network along with

the deactivation kinetics was previously reported as an enhanced calculation tool for this kind of processes [21].

The main goal of this work is to simulate the performance of different reactor configurations in catalytic processes with complex kinetic networks and fast deactivation. Ultimately, the most original aspect has been establishing a methodology for simulating these reactor configurations, and particularly fluidized bed reactors with catalyst circulation. We have taken the MTO process as representative example in order to explain the methodology and compare the performance of the different reactor configurations using a strategy that is based on analyzing both the catalytic activity and conversion.

2. Methodology

2.1. MTO kinetic model

The reaction network of MTO process has been deeply investigated and described with the dual-cycle mechanism [22,23], which relates the methylation and dealkylation of alkenes and aromatics from the simplified hydrocarbon pool mechanism [24]. Several detailed mechanistic kinetic models of this complex reaction have been reported [25–29]. However, none of them quantitatively consider the catalyst deactivation kinetics due to the complexity of its rigorous association with the steps of the mechanism. Alwahabi and Froment [30] established a simplified dependency of the SAPO-34 catalyst deactivation with the concentration of C_{6+} hydrocarbons. They assumed that these compounds are the main precursors of coke because they remain retained within the cages of the catalyst during the reaction. From these hypotheses, these authors

reported the design of three types of reactors: isothermal packed bed, adiabatic packed bed and bubbling fluidized bed reactors.

A more accurate consideration of catalyst deactivation is proposed by Janssens et al. [31]. Based on their previous observations, they attributed the formation of coke to the reaction of methanol with trimethylbenzene, highlighting the role of the aromatic cycle in the catalyst deactivation. Nevertheless, the indirect influence of olefins is also pointed out through its condensation toward aromatic structures and coke. More recently, Yuan et al. [32] proposed a lump kinetic model that simplifies the reaction network by differentiating only three groups of reactions ascribed to the olefin cycle, the conversion of olefins into aromatic and the aromatic cycle. The conversion of these active species (olefins and aromatics) into inactive ones (coke) describes the catalyst deactivation, whose parameters are estimated from experimental results of coke deposition.

In this study, the kinetic model used for the simulations was previously reported [33]. The kinetic network, based on the one described by Bos et al. [34] (**Table 1**), considers the individual formation of ethylene (C_2), propylene (C_3), butenes (C_4) and other hydrocarbons (paraffins and aromatics) from oxygenates (an equilibrium of methanol (M) and dimethyl ether (DME), **Eq. (1)-(4)**). The equations in **Table 1** do not have stoichiometric coefficient since they are expressed in terms of carbon units. Then, each C unit of the equilibrium M/DME is converted into a C unit of propylene, also forming water (W), according to **Eq. (3)**. The deactivation of the SAPO-34 catalyst is a consequence of coke formation and deposition, being its precursors all the components of the reaction medium (except for water, **Eq. (5)**).

Table 1. Reaction steps and kinetic constant values for each *j* reaction rate [33]

Reaction step		Kinetic equation	
Reaction network			
$M/DME \xrightarrow{k_1} C_2 + W$	(1)	$k_1 = 10.5 \exp\left[-\frac{98100}{R}\left(\frac{1}{T}-\frac{1}{698}\right)\right]$	(6)
$M/DME \xrightarrow{k_2} C_3 + W$	(2)	$k_2 = 13.7 \exp\left[-\frac{79000}{R}\left(\frac{1}{T}-\frac{1}{698}\right)\right]$	(7)
$M/DME \xrightarrow{k_3} C_4 + W$	(3)	$k_3 = 5.49 \exp\left[-\frac{59000}{R}\left(\frac{1}{T}-\frac{1}{698}\right)\right]$	(8)
$M/DME \xrightarrow{k_4} HC + W$	(4)	$k_4 = 1.00 \exp\left[-\frac{75000}{R}\left(\frac{1}{T}-\frac{1}{698}\right)\right]$	(9)
Deactivation kinetic			
$M/DME + C\text{-}prod \xrightarrow{k_d} coke$	(5)	$k_d = 229 \exp\left[-\frac{65300}{R}\left(\frac{1}{T}-\frac{1}{698}\right)\right]$	(10)

The rate of each step of the reaction network and the catalyst deactivation rate are described by the following equations:

$$\mathbf{r_j} = \frac{\mathbf{k_j} y_{OX}}{1 + K_W y_W} a \tag{11}$$

$$r_d = -\frac{k_d \left(y_{OX} + y_{C-prod}\right)}{1 + K_{Wd} y_W} a^2 \tag{12}$$

where $\mathbf{r_j}$ is the vector of the rates of each *j* reaction step in the reaction network and $\mathbf{k_j}$ is the vector of their kinetic constants (each one defined in **Table 1**). Both equations depend on y_{OX}, y_W and $y_{C\text{-}prod}$, which are the molar fraction of oxygenates (methanol + dimethyl ether), water and carbon-containing products (ethylene, C_2; propylene, C_3; butenes, C_4 and the rest of hydrocarbons, HC). The water adsorption constant K_W takes a value of 1.00, whereas K_{Wd} (in **Eq. (12)**) is defined as follows [35]:

$$K_{Wd} = 13.8 \exp\left[-\frac{58600}{R}\left(\frac{1}{698} - \frac{1}{T} \right) \right] \quad (13)$$

The catalyst deactivation is quantified by the activity (*a*), defined as the ratio between the reaction rate at *t* time and the reaction rate at zero time for the same reaction conditions available at *t* time. This is the required consideration in the analysis of the experimental data collected in an integral packed bed reactor for taking the "past history" of the catalyst into account [21,36]. According to the **Eq. (12)**, the deactivation kinetics is dependent on the concentrations of oxygenates and carbon-containing products in the reaction medium, which are the precursors of coke (**Eq. (12)**). Moreover, it considers the attenuating role of water (formed in the reaction (**Eqs. (1)-(4)**) or co-fed) in the formation of coke and catalyst deactivation [37–39]. This is a non-selective deactivation model, which considers the same activity in all the steps of the reaction network.

Most of the studies on deactivation kinetics during catalytic processes have related the catalyst activity to the content of coke, establishing trends of the activity drop with the increase in the formed coke or even to coke distributions on the catalyst particles [40,41]. The used deactivation equation (**Eq. (12)**) directly associates the activity with the operation conditions and time on stream [21]. This type of expressions has already been applied in the basic literature of reactor design [6–8] and presents several advantages over the coke-dependent kinetics. First, these latter assume that all carbonaceous species deposited on the catalyst surface contribute to deactivation without considering demonstrated factors as the aging of coke [42] or its nature and location [43–45]. In such a way, Gao et al. [14] reported the important effect of the location of coke on the reactant diffusion towards Brønsted acid sites and Muller et al. [46] studied the evolution with time of the nature of coke from oxygenated and higher-

deactivating species to lower-deactivating polyaromatic structures. Moreover, several authors provided further insights into the contribution of coke structures to the reaction mechanisms [47–49]. Secondly, reproducibility issues always exist when analyzing the content of coke of deactivated catalysts, mainly depending on the experimental protocol. Particularly, the previous sweeping or pretreatment of the samples (temperature and/or vacuum) has been reported as a crucial factor in the subsequent analysis [50]. Furthermore, the dependence of the longitudinal position in packed bed reactors [42] and the homogeneous distribution in fluidized ones [38,51] hinder the use of a unique coke content-based deactivation equation for all configurations. For all these reasons, we herein used a deactivation equation which does not directly depend on the content of coke, being able to compare the evolution of the activity in different reaction configurations.

The methodology used for computing the formation rate of each *i* lump, considering deactivation by coke, was previously proposed for the catalytic cracking of n-pentane [21]. All calculations are based on vectorized equations containing the above presented reaction rates. Thereby, let $\mathbf{r_L}$ be a column vector formed by the vector of the formation rates of each *i* lump ($\mathbf{r_i}$) and the catalyst deactivation rate (r_d). Also, let **r** be a column vector containing the vector of the rates of each *j* reaction step ($\mathbf{r_j}$) and the catalyst deactivation rate (r_d). Then, $\mathbf{r_L}$ and **r** vectors are related by a coefficient matrix (**A**) that contains the C and O balance coefficients:

$$\mathbf{r_L} = \begin{bmatrix} \mathbf{r_i} \\ r_d \end{bmatrix} = \mathbf{A}\,\mathbf{r} = \mathbf{A}\begin{bmatrix} \mathbf{r_j} \\ r_d \end{bmatrix}, \quad i = 1,...,n_l, \;\; j = 1,...,n_s \tag{14}$$

where **A** is defined as a matrix with $n_l + 1$ rows and $n_s + 1$ columns, being n_l and n_s the number of lumps and steps of the reaction network, respectively, and the additional row

and column ascribed to the deactivation kinetics ($\mathbf{A} = A_{n_l+1,n_s+1}$). In our particular case, considering the reaction network in **Table 1**:

$$\begin{bmatrix} r_{OX} \\ r_{C_2} \\ r_{C_3} \\ r_{C_4} \\ r_{HC} \\ r_{H_2O} \\ r_d \end{bmatrix} = \begin{bmatrix} -1 & -1 & -1 & -1 & 0 \\ 1 & 0 & 0 & 0 & 0 \\ 0 & 1 & 0 & 0 & 0 \\ 0 & 0 & 1 & 0 & 0 \\ 0 & 0 & 0 & 1 & 0 \\ 1 & 1 & 1 & 1 & 0 \\ 0 & 0 & 0 & 0 & 1 \end{bmatrix} \begin{bmatrix} r_1 \\ r_2 \\ r_3 \\ r_4 \\ r_d \end{bmatrix} \tag{15}$$

2.2. Conservation equations

All reactor models were described with the conservation equations of the molar fractions of each *i* lump (in terms of C units) and of the catalyst activity. Isothermal reactors and ideal flows for the gas and solid were considered, with the aim of comparing the activity profiles along the longitudinal position and their evolution with time. The reason is to avoid masking the effect of activity by differences of temperature or by real flow characteristics. The system is then described by the convection-dispersion-reaction equation for one-dimensional gas and solid flows. Considering a vector of molar fractions $\mathbf{y_i}(z,t)$ and a catalyst activity $a(z,t)$:

$$\varepsilon_b \frac{\partial}{\partial t}\mathbf{y_i}(z,t) = \frac{\partial}{\partial z}\left[-v\mathbf{y_i}(z,t) + D\frac{\partial}{\partial z}\mathbf{y_i}(z,t)\right] + \frac{RT}{PN_C}\rho_b \mathbf{r_i}, \quad i = 1,...,n_l \tag{16}$$

$$\frac{\partial}{\partial t}a(z,t) = \frac{\partial}{\partial z}\left[-v_{cat}a(z,t) + D_{cat}\frac{\partial}{dz}a(z,t)\right] + r_d \tag{17}$$

defined for $t > 0$ and $0 < z < L$, and where ε_b is the effective bed-particle porosity, v is the linear velocity, D is effective dispersion coefficient of the gas, R is the universal gas constant, T is the reactor temperature, P is the total pressure, N_C is the (carbon molar flow rate)/(total molar flow rate) ratio, ρ_b is the catalytic bed density, v_{cat} is the linear

velocity of the catalyst particles, D_{cat} is the dispersion coefficient associated to the particle movement, r_d is the catalyst deactivation rate and L is the catalytic bed length. As we above presented, activity is defined as a ratio between reaction rates at different times but same reaction condition. In this approach, the dimensionless character of activity is used for considering the balance of active sites. Activity is assumed as the ratio of the remaining active sites in the catalyst and the total amount of them (active and deactivated). This mathematical tool allows a computationally fast and understandable approach to describe the solid regime in different reactor configurations without assuming excessively high errors.

The effective dispersion coefficient for the gas flow was calculated from the Peclet (*Pe*) number (**Eq. (18)**) assuming high enough values for a practically convective gas flow [52]. Note that the presence of the diffusive term turned out to be required in **Eq. (16)** for the stability of the calculation methodology in spite of its negligible value [21].

$$Pe = \frac{Lv}{D} \tag{18}$$

Likewise, the convection and dispersion terms for the catalyst particles are related by the Bodenstein number (*Bo*) in reactor configurations with catalyst circulation (moving or fluidized bed) [52,53].

$$Bo = \frac{Lv_{cat}}{D_{cat}} \tag{19}$$

This parameter quantifies the contribution of the convective and dispersive transport of a particle in a catalytic bed of L length [54]. Thus, ideal solid regimes of plug flow and CSTR are respectively reached when $Bo \rightarrow \infty$ and $Bo \rightarrow 0$. Consequently, high values of *Bo* ($>10^2$) mean negligible dispersion of the activity and thus regimes with package catalyst particles. Otherwise, low values of *Bo* ($<10^{-5}$) indicates an almost perfect mix of

the activity along the catalytic bed and then ideal fluidized bed regimes. Therefore, this is the crucial parameter for defining the solid regime. **Table 2** summarizes the values of the gas and solid linear velocities (v and v_{cat}, respectively) and dispersion coefficients (D and D_{cat}, respectively), which define the convection and dispersion terms of **Eq. (16)** and **Eq. (17)**. The studied reactor configurations are schematized in **Fig. 1**. In all cases, the gas is assumed to present an ideal non-dispersive plug flow regime, being the linear velocity calculated from the reactant flow rate in terms of contained carbon (υ_o) and the reactor section (S). The description of the different solid regimes of **Fig. 1** requires modifications in the convection and dispersion terms of **Eq. (17)**.

Table 2. Definition of the convection and dispersion terms in **Eqs. (16)** and **(17)** for gas flow and solid regime in the different reactor configurations

Convection term		**Dispersion term**	
Gas flow			
$v = \frac{\upsilon_o}{S}$	(20)	$D \to 0$	(21)
Solid regime			
Packed bed reactor (PBR)			
$v_{cat} = 0$	(22)	$D_{cat} = 0$	(23)
Moving bed reactor (MBR)			
$v_{cat} = \pm\frac{L}{\tau}$	(24)	$D_{cat} \to 0$	(25)
Non-circulating fluidized bed reactor (NCFBR)			
$v_{cat} \to 0$	(26)	$D_{cat} \to \infty$	(27)
Circulating fluidized bed reactor (CFBR)			
$v_{cat,r} = \frac{q_{cat}}{n_r S_r}$	(28)	$D_{cat} \to \infty$	(29)

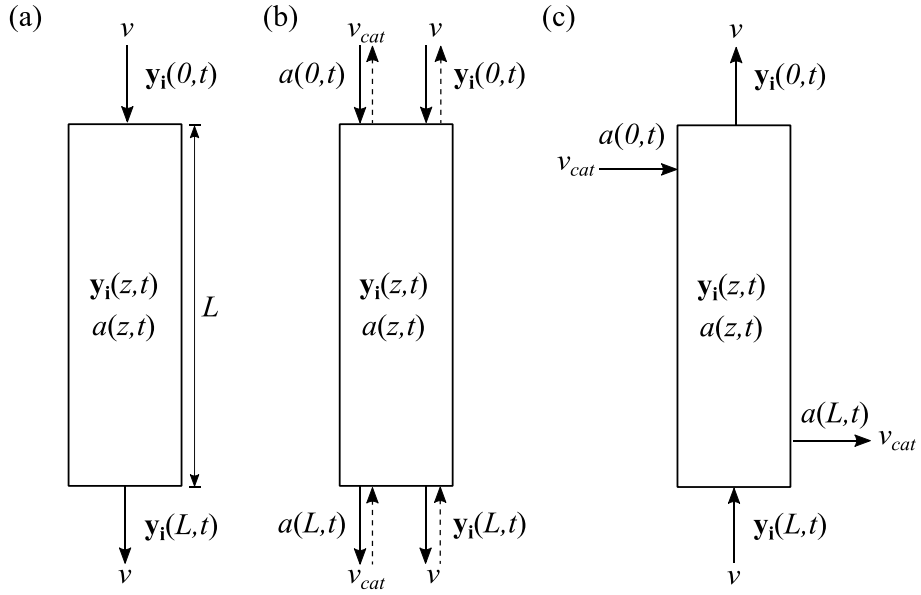

Fig. 1. Schemes of the (a) packed bed, (b) moving bed and (c) fluidized bed reactor configurations

2.3. Packed bed reactor

The packed bed reactor (PBR) is the more elementary and easy to handle configuration of **Fig. 1**. For this reason, it is the main configuration operated at laboratory scale in order to collect experimental data and compute kinetic models, as the one used in this work (**Table 1**). The catalyst particles are packaged (**Fig. 1a**), and then v_{cat} and D_{cat} are null (**Table 2**). The convection-dispersion-reaction equation for activity (**Eq. (17)**) is reduced to the source term, and therefore, the evolution of the activity with time corresponds to the deactivation rate (r_d).

2.4. Moving bed reactors

Moving bed reactors (MBR, **Fig. 1b**) are suitable in cases in which the production is required constant but the catalyst deactivation is relatively fast. The MTO process using a HZSM-5 zeolite could be considered as an example of these processes, where the deactivation is slower than that registered with a SAPO-34 catalyst [17]. An ideal non-

dispersive movement of the catalyst particles is assumed in order to describe the moving bed regime (plug flow model). For a given reactor section (S) and assuming constant the bed density (ρ_b), the linear velocity of the catalyst (v_{cat}) can be defined as a function of the residence time (τ) of a particle in the catalytic bed (**Table 2**). In this case, two different configurations must also be differentiated depending on the direction of the gas and solid flows: co-current or counter-current. This determines the positive or negative value of v_{cat} indicated in **Table 2**. As an example of this reactor configuration, the riser (FCC) corresponds to the particular case of co-current MBR (**Fig. 1b**) in which gas and solid flows have equal and very low residence time (< 5 s). Likewise, downer reactors present a descending solid flow and allow operating with co-current (descending) or counter-current (ascending) gas flow [55,56].

2.5. Fluidized bed reactors

The main advantage of fluidized bed reactors (**Fig. 1c**) is the fact that isothermal conditions are obtained easier than the rest of configuration. This happens in exothermic reactions, as the ones in MTO process, as well as in endothermic reactions. Moreover, the particle movement enable to circulate the catalyst particles continuously (if desired) in order to ensure steady yields if the catalyst is regenerated. Again, the gas flow is assumed to follow an ideal plug flow regime, and a uniform activity in the whole bed should be taken into account for the reactor design according to the ideal random movement of particles [51]. This means a *Bo* value so low as the dispersion of the catalyst activity would tend to very high values (**Table 2**). Two kinds of fluidized bed reactors must be differentiated depending of the catalyst particles circulation: non-circulating or circulating fluidized bed reactors (NCFBR and CFBR, respectively). Based on that, the v_{cat} is negligible in the case of NCFBR (theoretically infinite residence time for solids).

Contrary to the behavior of a moving bed reactor in which all particles in the bed are homogeneously moved, the design of CFBR is conditioned by the existence of a residence time distribution (RTD) of catalyst particles, associated with the perfect mixing of solids in a bubbling fluidized bed [57,58]. Then, the catalyst deactivation would lead to an activity distribution that must be taken into account. This RTD profile is given by the *E* curve and can be expressed as a function of the evolution of the activity with time [59,60]:

$$f_a(t) = \frac{E(\tau)}{-\frac{d}{dt}a(z,t)} \tag{30}$$

The hereby presented model proposes an original approach to consider the RTD of particles based on a system of parallel compartments with catalyst circulation (**Fig. 2**), all of them in a fluidized regime. For accomplishing that, a discretization of the *E* curve was carried out (**Fig. S1**) by dividing the catalyst particles in groups with the same residence time. Thereby, let n_r be the number of particle groups and let τ_r be the residence time of each *r* particle group, then, the CFBR is described by the n_r parallel compartments depicted in **Fig. 2**.

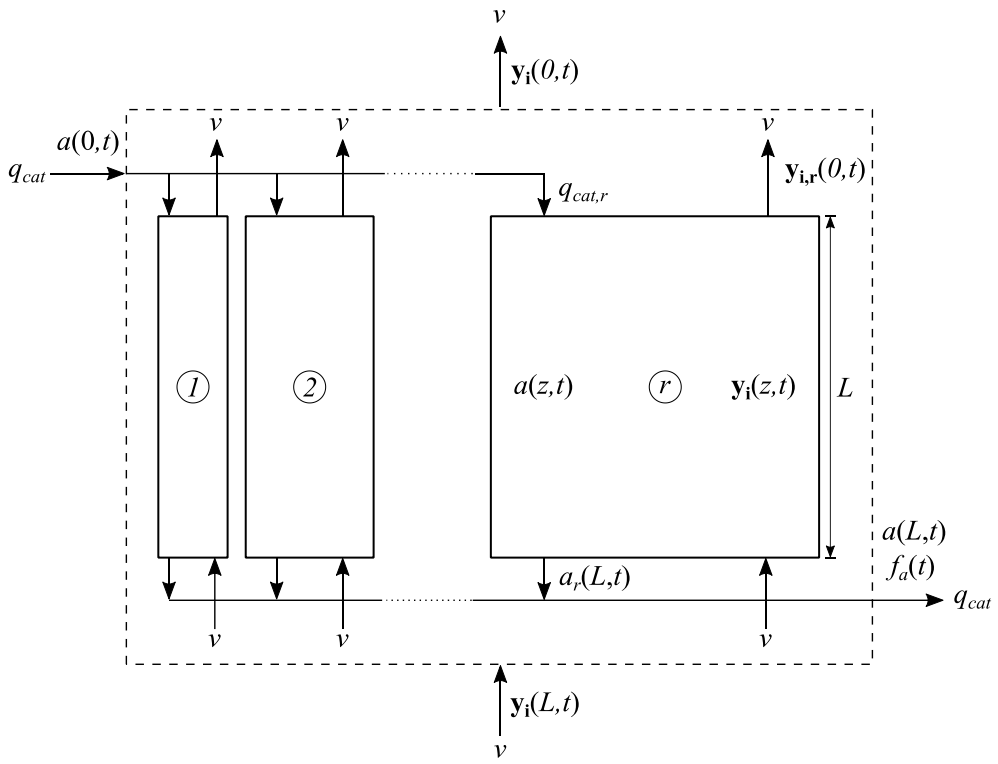

Fig. 2. Model of parallel compartments for describing a circulating fluidized bed reactor

Note that the section of each compartment (S_r) in **Fig. 2** is different, as well as the relative velocity between gas and solid, being constant the gas linear velocity (v) and the catalyst flow rate ($q_{cat,r}$), and fulfilling:

$$q_{cat,r} = \frac{q_{cat}}{n_r} = v_{cat,r} S_r \tag{31}$$

where q_{cat} is the total catalyst flow rate, $v_{cat,r}$ is the linear velocity of the catalyst in each compartment (used parameter in **Eq. (17)**) and S_r fulfills:

$$S = \sum_{r=1}^{n_R} S_r \tag{32}$$

Taking these assumptions into consideration, the gas molar flow rate (in terms of carbon) is distributed in each compartment depending on its section (S_r):

$$F_r = \frac{vPS_r}{RT} \tag{33}$$

where F_r is the molar flow rate in terms of carbon in each reactor, and then at the inlet/outlet of the reactor the next equation must also be fulfilled:

$$F = \frac{vPS}{RT} = \frac{vP}{RT}\sum_{r=1}^{n_R} S_r \tag{34}$$

where F is the total molar flow rate in terms of contained carbon.

The resolution of each reactor conservation equations, given by **Eqs. (16)** and **(17)** and the parameters in **Table 2**, requires the initial and boundary conditions listed in **Table 3**. Due to the presence of the dispersion term in the gas conservation equation, Robin (instead of Dirichlet) and Neumann boundary conditions were used at the inlet and at the outlet of the reactor, respectively. In the case of the catalyst particles, the same Robin and Neumann boundary conditions were used in regimes with solid movement. Note that the PBR does not require boundary conditions (**Eq. (17)** is only time-dependent in this case) and the ones of co-current MBR and counter-current MBR change as a function of the direction of gas and solid flows. Using these initial and boundary conditions, the resulted system of partial differential equations (PDEs) was solved using a developed vectorized calculation method that transform each PDE into ordinary differential equations (ODEs) by the finite differential method proposed by Skeel and Berzins [61]. Once transformed, the system of ODEs was integrated using an implicit Runge-Kutta solver based on the numerical differentiation formulas of orders 1 to 5. The routine was implemented in MATLAB using the *ode15s* solver.

Table 3. Initial and boundary conditions for each reactor model

Initial conditions		**Boundary conditions**	
$\mathbf{y_i}(z,0)=\mathbf{y_0}$	(35)	$-v\left[\mathbf{y_i}(0,t)-\mathbf{y_0}\right]+D\frac{\partial}{\partial z}\mathbf{y_i}(0,t)=0$	(36)
		$\frac{\partial}{\partial z}\mathbf{y_i}(L,t)=0$	(37)
Fixed bed reactor			
$a(z,0)=1$	(38)		
Moving bed reactor			
$a(z,0)=1$	(39)	$-v_{cat}\left[a(0,t)-1\right]+D_{cat}\frac{\partial}{\partial z}a(0,t)=0$ [a]	(40)
		$\frac{\partial}{\partial z}a(L,t)=0$	(41)
Fluidized bed reactor			
$a(z,0)=1$	(42)	$-v_{cat}\left[a(0,t)-1\right]+D_{cat}\frac{\partial}{\partial z}a(0,t)=0$ [b]	(43)
		$\frac{\partial}{\partial z}a(L,t)=0$	(44)

[a] $a(L,t)$ in the case of counter-current MBR

[b] $v_{cat,r}$ for each compartment in the case of CFBR

3. Results and Discussion

From the above introduced methodology, the evolution with time and reactor longitudinal position can be predicted for each reactor configuration. Based on this, the results are divided in different sections: packed bed reactor (PBR, section 3.1), moving bed reactor (MBR, section 3.2), non-circulating fluidized bed reactor (NCFBR, section 3.3) and circulating fluidized bed reactor (CFBR, section 3.4). Initial results of activity and conversion (t = 5 10^{-3} h) along the longitudinal position of the reactor, as well as their evolution with time at the reactor outlet ($z = L$), are depicted for configurations without catalyst circulation (PBR and NCFBR), whereas results of the steady state values are given for those with catalyst circulation (MBR and CFBR). Finally, the scope and applications of the methodology are summarized in the section 3.5.

3.1. Packed bed reactor

The performance of a packed bed reactor (PBR) in the MTO process was simulated by using the **Eqs. (16)** and **(17)** with the conditions indicated in the **Table 2**. **Fig. 3** shows the activity and conversion profiles along the longitudinal position z and their evolutions with time at the reactor outlet ($z = L$). The results for each temperature (648, 698 and 748 K) are shown, as well as the effect of diluting the methanol feed with water (water/methanol ratio, W/M = 1 and 3) at 698 K. **Fig. 3a** shows the initial longitudinal profiles ($t = 5\ 10^{-3}$ h) of activity that exhibit a minimum at the inlet of the reactor ($z = 0$). This minimum value is lower upon increasing the temperature and is attributed to the lower concentration of water at $z = 0$ [51]. This is consistent with the deactivation equation (**Eq. (12)**) in which the activity decay is proportional to the concentration of all C-containing components of the reaction medium and inhibited by the presence of water (inexistent at the inlet of the reactor for W/M = 0). Interestingly, the activity profile drastically changes when water is fed with methanol, and the initial minimum is significantly softened (see dashed lines in **Fig. 1a**). At $t = 5\ 10^{-3}$ h and the same reaction conditions, the longitudinal profiles of conversion in **Fig. 1b** correspond to the computed activity profiles in **Fig. 1a**. As expected, the methanol conversion is negligible at the inlet of the reactor ($z = 0$) and maximum at the outlet and the highest temperature. In the same way, the initial conversion of methanol decreases when water is fed. This also highlights the role of water in the attenuation of reaction rates taken into account in the MTO kinetic model (**Table 1**). The predicted olefin distributions at the outlet of the reactor at these conditions are detailed in **Fig. S2a**. In all cases, propylene is the main product of the reaction nearly followed by ethylene and butenes.

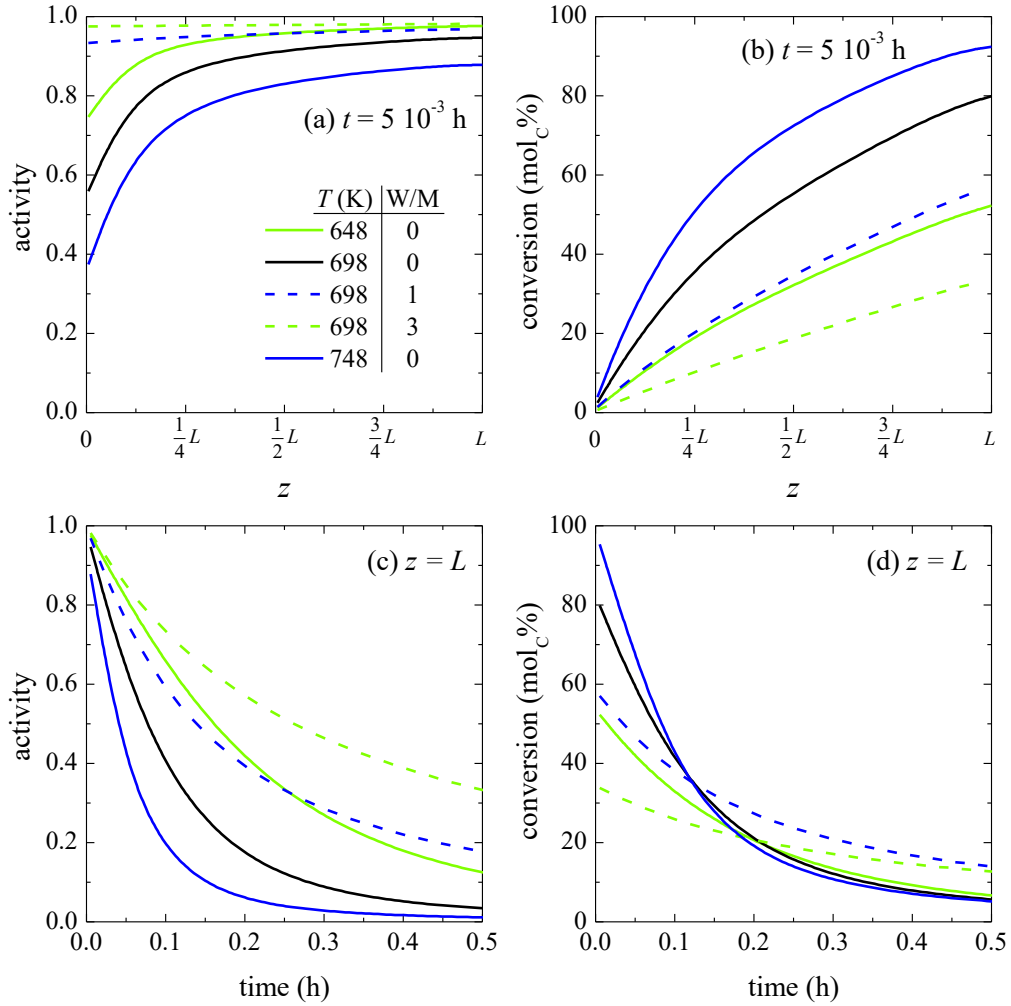

Fig. 3. Effect of temperature and co-feeding water on the initial ($t = 5\ 10^{-3}$ h) longitudinal profiles of (a) activity and (b) conversion and on the evolution with time of (c) the activity and (d) the conversion at the reactor outlet (z = L) in a PBR. Conditions: space time, 0.1 $g_{catalyst}$ h mol_C^{-1}; T, 648–748 K, W/M, 0–3 (698 K)

The evolution with time of the activity at $z = L$ is observed in **Fig. 3c**. According to the results, a faster activity drop is shown upon increasing the temperature (from 698 to 748 K) and an increase in the amount of co-fed water slows down the deactivation rate. It is noteworthy the increase in the activity from 0.03 to 0.32 with a W/M ratio of 3 after 0.5 h. The evolution with time of the conversion computed with these activity values

follows similar trends with temperature and W/M ratio (**Fig. 3d**). From these results, it can be stated that high temperatures and low water content lead to high conversions at low time on stream values but faster catalyst deactivation. On the other hand, a decrease in the temperature or an increase in the amount of co-fed water makes the initial conversion drop but softens the deactivation rate, which could enlarge the catalyst lifetime [39]. A similar trend is followed by the olefin yields (**Fig. S2b**), whose drops with time are similar to those of conversion at all conditions. The herein simulated results for a PBR are in good agreement with the experimental results previously reported by our research group [33] and thereby, the simulation methodology can be considered as a valid tool for a reliable reproduction of experimental data collected at laboratory scale.

3.2. Moving bed reactor

Similar to the PBR, design equations for a moving bed reactor (MBR) provide longitudinal profiles of activity and conversion and their evolutions with time. In this case, the model predicts an initial transitory state in which the reaction reaches an operational steady state. **Figs. S3a** and **S3b** show these evolutions of the activity and conversion, respectively. A crucial parameter for designing this reactor is the residence time of the catalyst (τ), defined as the time that a particle spends inside the catalytic bed, which is controlled by the catalyst mass flow rate. Considering negligible dispersive transport of the catalyst in any case ($Bo \rightarrow \infty$), two different τ values (0.1 and 0.5 h) and different reaction conditions were simulated in a co-current MBR. As observed in **Fig. S3**, the steady state is by far reached in all cases after 1 h.

Fig. 4 displays the steady state longitudinal profile of activity (**Fig. 4a**) and the conversion values at the outlet of the reactor in this steady state (**Fig. 4b**). Maximum activity values are observed at $z = 0$ as the catalyst is fed at the inlet of the reactor with

values of activity of 1 (**Fig. 4a**). Similar to the performance of the PBR, an increase in the temperature leads to more pronounced activity drops and the presence of water attenuates them. Moreover, the model predicts that catalyst deactivation is more remarkable upon increasing τ. Regarding the conversion at the outlet of the reactor ($z = L$, **Fig. 4b**), higher values are predicted for $\tau = 0.1$ h, following the same trend that the one previously observed for PBR (**Fig. 3d**). Interestingly, increasing τ up to 0.5 h a maximum conversion of 27% is obtained at the lowest depicted temperature (698 K) and co-feeding water (W/M = 1). Although the initial conversion is significantly lower (**Fig. S3**), the slower deactivation of the catalyst with water leads to a steady state in which the activity profile is higher (**Fig. 4a**), thus resulting in higher conversion values (**Fig. 4b**).

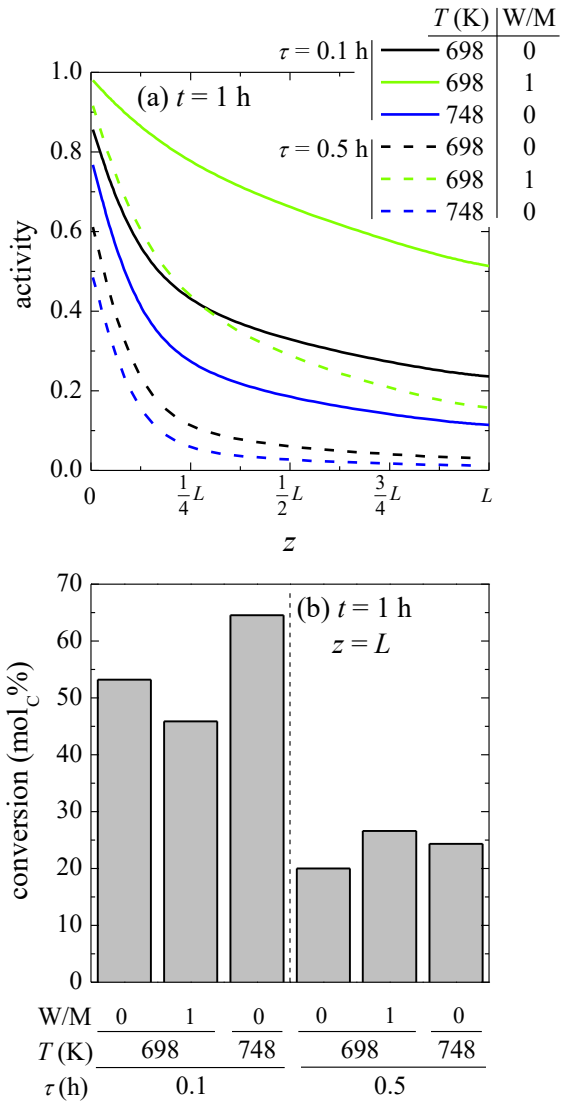

Fig. 4. Effect of the residence time of the catalyst on the steady state longitudinal profiles of (a) activity and (b) conversion values at the reactor outlet ($z = L$) in a co-current MBR. Conditions: space time, 0.1 $g_{catalyst}$ h mol_C^{-1}; T, 698–748 K, W/M, 0–1 (698 K)

As it is previously explained (**Fig. 1)**, this reactor configuration allows changing the direction of gas and solid flows, which causes interesting modifications of the reactor performance. Once reached the steady state, the longitudinal profiles of activity and the conversion values at $z = L$ of both are compared in **Fig. 5a** and **Fig. 5b**, respectively.

Note that the fresh catalyst is fed at $z = L$ in a counter-current MBR, which explains the opposite evolution of the activity with z. In a case of concentration-independent deactivation equation, these profiles should be symmetric and the intersection point should coincide with $z = 1/2L$. This is not our case and a strong influence of the direction of gas and solid flows is observed. Regarding the simulations without co-feeding water, a more pronounced deactivation is observed in the co-current MBR near $z = 0$, which is attenuated along z. This leads to higher values of conversion at $z = L$ (**Fig. 5b**) for the countr-current MBR. Indeed, counter-current MBR allows for obtaining similar conversion values (ca. 65%) using a temperature of 50 K lower. Again, water plays an important role in the process and the inhibition of both, reaction and deactivation rates, tends to equalize the activity profiles in both cases (makes them more symmetric). High water concentration gives relevance to the denominator of **Eq. (11)** and **Eq. (12)**, which approaches reaction and deactivation rates to concentration-independent equations. As a consequence, almost the same conversions are predicted in both cases at the steady state (**Fig. 5b**).

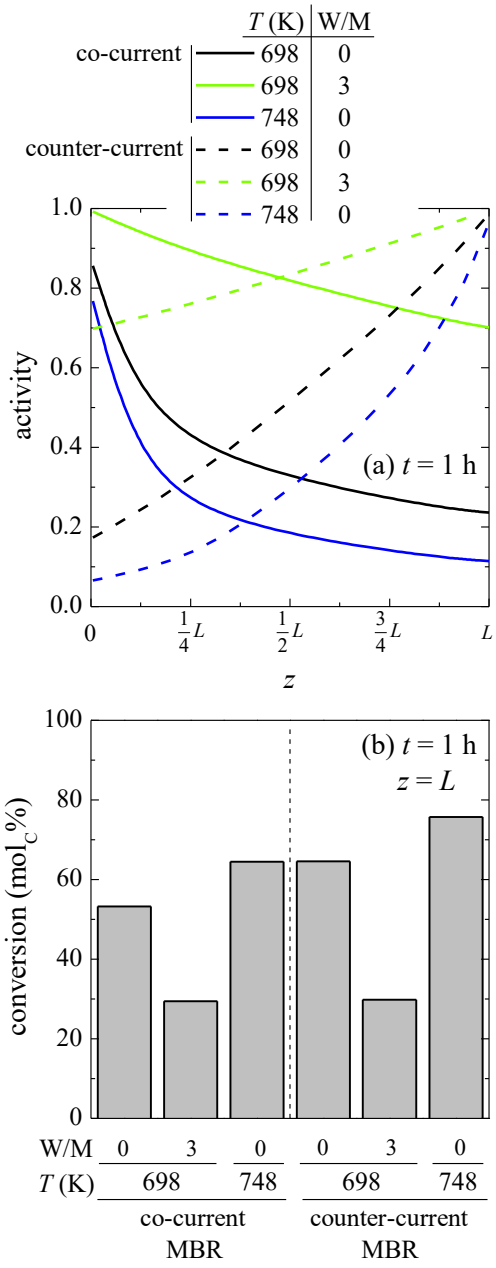

Fig. 5. Effect of the direction of gas and solid flows in a MBR on the steady state longitudinal profiles of (a) activity and (b) conversion values at the reactor outlet ($z = L$). Conditions: space time, 0.1 $g_{catalyst}$ h mol_C^{-1}; T, 698–748 K, W/M, 0–3 (698 K); τ, 0.1 h

3.3. Non-circulating fluidized bed reactor

From a computational point of view, just a change in the the D_{cat} parameter, which characterize the catalyst dispersion in the design equation (**Table 2**) allows for simulating a completely different reactor configuration. An ideal non-circulating fluidized bed reactor (NCFBR) is described by a gas flow following a plug flow regime and completely mixed catalyst particles. The case of NCFBR without catalyst circulation can be understood as a catalytic bed in which all the particles present the same activity. This ideal performance is well-predicted in the simulations (**Fig. 6a**) in contrast to the defined profiles predicted for a PBR (dashed lines). In this comparison, the harsher the reaction conditions, the more different are the performances of both configurations. Hence, the greatest differences are observed at 748 K, achieving slightly higher initial conversions (at $t = 5\ 10^{-3}$ h) with the NCFBR (**Fig. 6b**). Nevertheless, the attenuation of reaction and deactivation rates by water tends to make equal the conversion attained in both cases as the longitudinal profile of activity is significantly softened. For comparing the evolution of the activity with time in both reactors, three different z points are analyzed at a given reaction conditions in order to understand the main distinction in these two reactors (**Fig. 6c**). Certainly, the same evolution with time is followed by all the particles in a NCFBR because of the particle ideal mixing. However, this does not happen in the case of the PBR. At $z = 0$, a much lower initial activity and a faster deactivation are observed than those for the NCFBR. Otherwise, a slightly higher initial value and slower deactivation are registered at $z = L$. As a consequence, the evolution with time of the conversion at the outlet of the reactor is predicted similar **(Fig. 6d)**.

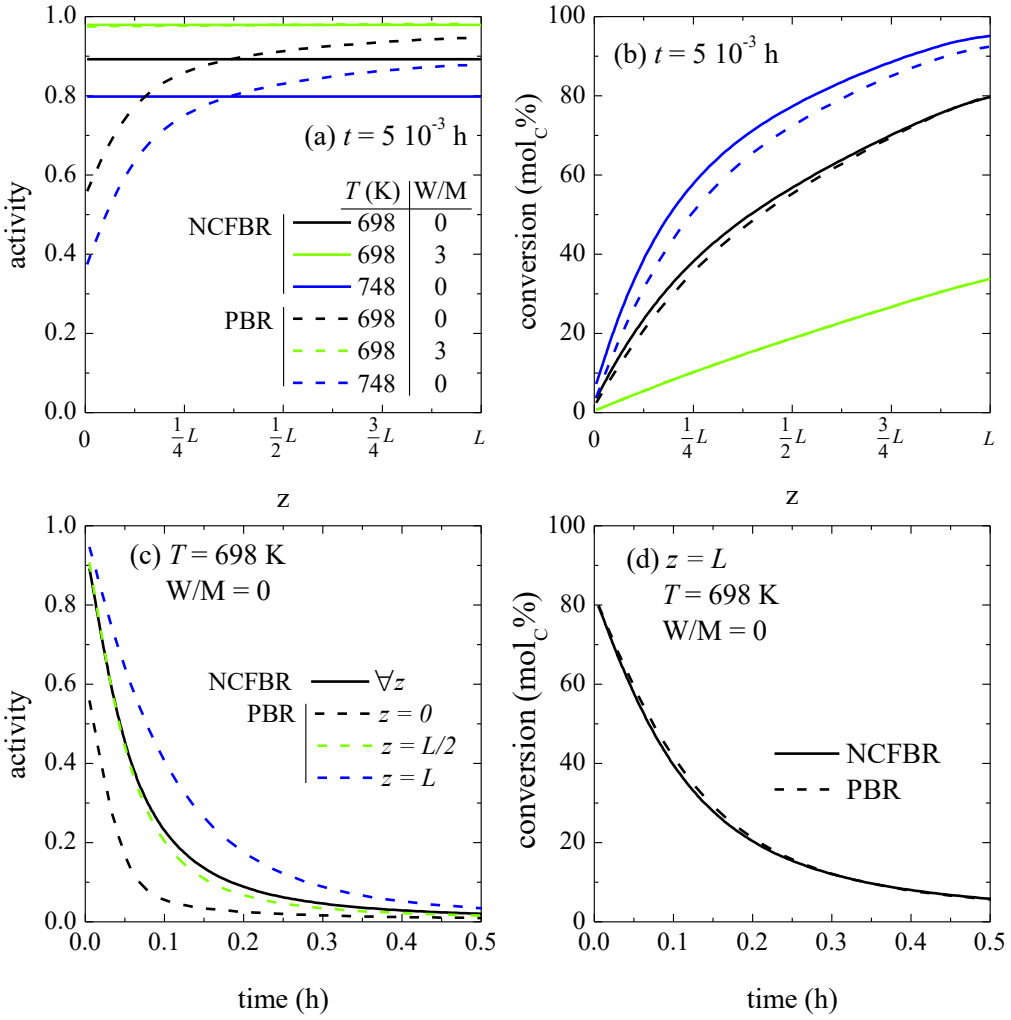

Fig. 6. Comparison between the initial ($t = 5\ 10^{-3}$ h) longitudinal profiles of (a) activity and (b) conversion and the evolution with time of (c) the activity at different reactor positions and (d) the conversion at the reactor outlet ($z = L$) for NCFBR and PBR configurations. Conditions: space time, 0.1 $g_{catalyst}$ h $molC^{-1}$; T, 698–748 K, W/M, 0–3 (698 K)

3.4. Circulating fluidized bed reactor

The proposed parallel compartments approach (**Fig. 2**) can offer a simple way for understanding the concept of catalyst particles with different residence times in a

circulating fluidized bed reactor (CFBR), as it is explained in detail in section 2.5. However, the calculation requires a minimum number of compartments (n_R in **Fig. 2**) in order to achieve reproducible simulation results. This is a numerical issue that currently happens in models in which a discretization of variables is involved, in our case the RTD profile (**Fig. S1**). For this reason, simulations with different number of compartments (5, 10, 50 and 100) were carried out. **Figs. S4a-c** show the activity distribution functions (f_a) of catalyst particles at the outlet of the reactor at 5 10^{-3}, 5 10^{-2} and 1 h, respectively. As indicated in **Table 3**, a uniform activity is considered at the inlet of the reactor ($a(0,t)=1$). The evolution of the conversion with time in each case is depicted in **Fig. S4d**. At the beginning of the simulations, when high values of activity and narrow distributions are observed, the results are similar in all cases (**Fig. S4a**). Nevertheless, the influence of the number of compartments is shown for wider activity distributions. Indeed, five well-defined peaks are observed for $n_R = 5$ that correspond to the activity at the outlet of each compartment. Although this indicates that the calculation is computationally correct, this result does not reproduce the real performance of a CFBR. Therefore, n_r must be higher. Regarding the evolution of the activity distribution function and the conversion with time, it could be stated that the results obtained with 50 and 100 compartments are practically reproducible (see the inset of **Fig. S4d**). Since operations with 50 compartments are computationally cheaper, this value ($n_r = 50$) is selected as an appropriate one for performing the simulations of a CFBR.

From the results of **Fig. S4**, it can be deduced that the movement of catalyst particles in the CFBR leads to a steady state of activity and conversion, as observed before with the MBR. **Fig. S5** shows the evolution of the activity distribution function and conversions with time at different reaction conditions, including the mean residence time of the

catalyst (τ_m). In all cases, the steady state is reached before 1 h of simulation. Hence, the results of the simulations of the CFBR in **Fig. 7** are depicted for this operation time. **Fig. 7a** and **Fig. 7b** show the activity distribution function predicted by the model at different reaction conditions using τ_m values of 0.1 and 0.5 h, respectively. Comparing both figures, a strong influence of τ_m is observed, being the activity distribution function shifted toward lower activity values upon increasing the mean residence time of the catalyst. Indeed, a variation in τ_m for a given reaction condition (698 K and W/M = 0) modifies the activity distribution function, predicting displacements of the maximum location from activity values of 1 to 0.08 (**Fig. S6**).

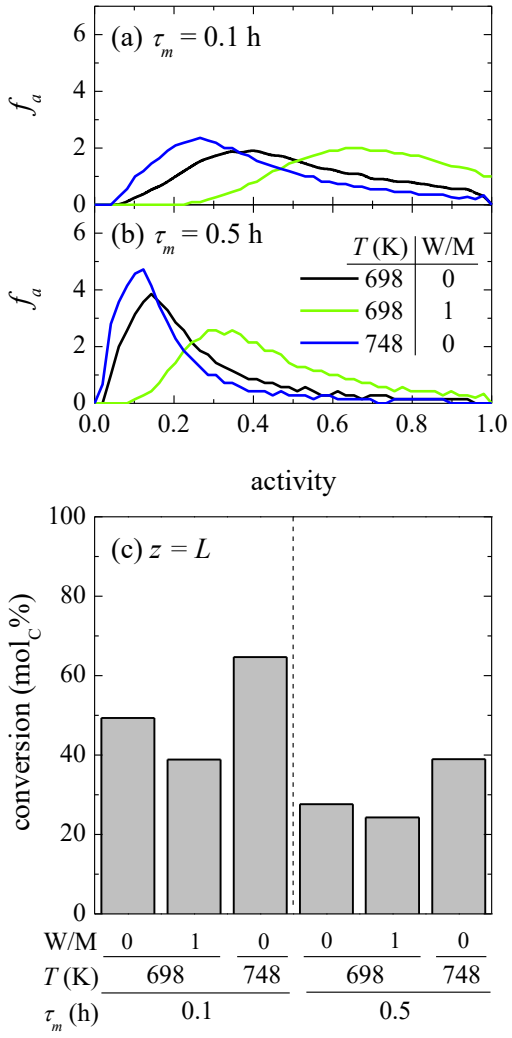

Fig. 7. Effect of temperature and co-feeding water on the activity distribution function with mean residence time values of (a) 0.1 and (b) 0.5 h and on the steady state (c) conversion at the reactor outlet ($z = L$) in a CFBR. Conditions: space time, 0.1 $g_{catalyst}$ h mol_C^{-1}; T, 698–748 K, W/M, 0–1 (698 K)

In both **Figs. 7a** and **7b**, the increase in the temperature leads to a displacement of the activity distribution function towards lower values of activity, whereas co-feeding water softens the catalyst deactivation, then registering activity distribution functions with maxima at higher activity values. In terms of conversion (**Fig. 7c**), an increase in the temperature means higher conversion values, whereas the presence of water leads to a decrease of the steady state conversion. As it was also observed with the MBR, the lower the residence time of the catalyst, the lower deactivation of the catalyst is predicted, which allows obtaining higher conversion values.

3.5. Scope of the methodology

From an industrial point of view, the original design of reactors with catalyst circulation can be an attractive tool for analyzing the feasibility of processes already commercialized or in development state [62]. Some of them have already been proposed to be carried out in MBR for dealing with catalyst deactivation, for instance the catalytic reforming of naphtha [63], the isobutane dehydrogenation [64] or the steam reforming of methane [65]. However, the clearest example can be found in the FCC unit, which is the core of a refinery and uses MBR for both reactor (riser) and striping sub-unit with ascendant and descendant catalyst flow, respectively [66]. The third main part of this unit, the regenerator sub-unit, operates under CFBR conditions, which could also be modeled with this methodology by developing the reactivation kinetic model and assuming an ideal mixing of the catalyst particles [67]. This CFBR configuration are

also reported for some already established processes at pilot plant or laboratory scale such as, gasification/pyrolysis of biomass [68] or the herein studied MTO process [5].

Once given its kinetic model, the simulation and comparison of different reactor configurations for a catalytic process is one of the easy possibilities offered by this methodology. Then going back to our MTO process, a comparison of the performance of different reaction configurations with circulation of the catalyst particles was made, and the predicted conversion at the steady state with the co-current MBR, counter-current MBR and CFBR are displayed in **Fig. 8a** and **Fig. 8b** for $\tau = 0.1$ and 0.5 h, respectively (τ_m in the CFBR). **Fig. S7** also details the olefin distribution in each case. At 698 K and without co-feeding water, counter-current MBR provides higher conversion and yields of olefins than co-current MBR (as discussed above, **Fig. 5**), being CFBR the worst configuration. However, at 748 K the conversion and yields of olefins predicted with the CFBR are similar to those with co-current MBR. This points out the effectiveness of fluidized bed reactors at conditions of fast deactivation and is related to the significant differences in the activity profiles also observed for PBR and NCFBR (**Fig. 6a**). Not to mention, the fact that it is easier to reach an isothermal state in a CFBR than in a PBR. Interestingly, the incorporation of water in the reaction medium equalizes the conversions and yields of olefins of both MBRs but maintains lower ones in the CFBR. This trend is also observed for higher values of residence time (**Figs. 8b** and **S7**) when the incorporation of water makes the CFBR the worst reactor configuration (in terms of conversion and yields) despite at this condition of high deactivation, it exhibits the best performance when pure methanol is fed at 698 and 748 K.

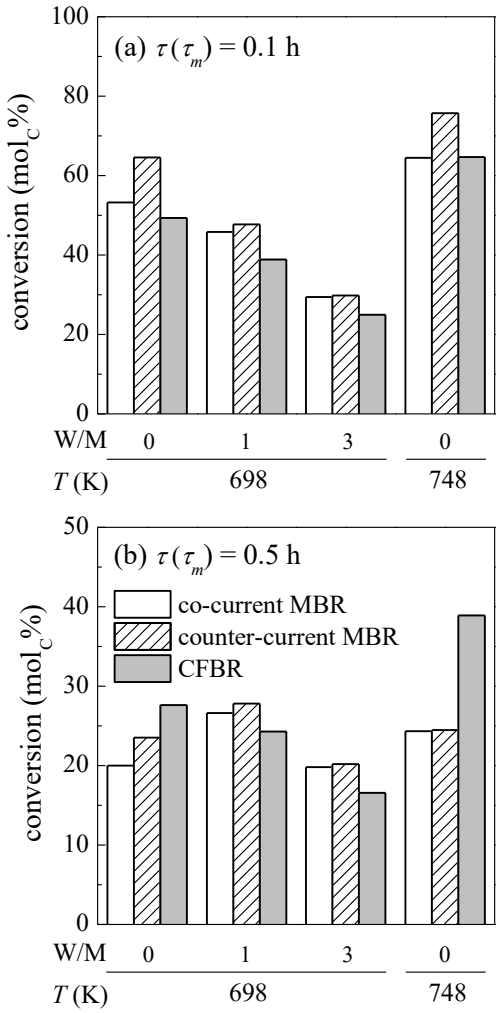

Fig. 8. Comparison of the steady state conversion values with co-current MBR, counter-current MBR and CFBR for (mean) residence time of (a) 0.1 and (b) 0.5 h. Conditions: space time, 0.1 $g_{catalyst}$ h mol_C^{-1}; T, 698–748 K, W/M, 0–3 (698 K)

Our methodology also allows providing interesting results regarding screening of catalysts by analyzing their performance in each reactor configuration. In previous work, we have validated experimental data and developed kinetic models for MTO (methanol-to-olefins) and DTO (dimethyl ether-to-olefins) processes over SAPO-34 [33] and ZSM-5 catalysts [20], including the catalyst deactivation. Adaptations of these models have been used for studying the effect of the catalyst on each of the reactor

configurations. **Table S1** shows the kinetic parameters and deactivation equations of each kinetic model and **Fig. S8** depicts some selected results on the performance of these catalysts in each reactor configuration. In this particular case, it can be clearly observed that SAPO-34 catalyst exhibits higher conversions than ZSM-5 catalyst (**Fig. S8b**). However, this latter shows a slower deactivation in a NCFBR (**Fig. S8c**), which leads to lower deactivated catalyst degrees in reactor configurations with catalyst circulation (**Fig. S8d** and **S8e**). As expected, the product distribution is remarkably different (**Fig. S8f**), being worth of mentioning the higher yield of long hydrocarbons (HC) with ZSM-5 catalyst. Indeed, this catalyst has been reported as the most suitable for MTG (methanol-to-gasoline) process [31].

Based on these results, and assuming that the implementation of these processes with fast deactivation (such as MTO with SAPO-34 catalyst) requires the circulation of the catalyst for its regeneration, the optimum predicted reactor configuration depends on the catalyst activity and reaction conditions. Hence, moving bed reactors allow for operating with short residence time values and co-feeding water that enlarge the catalyst lifetime. On the other hand, circulating fluidized bed reactors are the suitable choice for longer mean residence times and conditions of fast deactivation. Despite an accurate comparison of these reactor configurations is allowed by the proposed methodology, further studies considering energy conservation equations and non-ideal flows should be taken into account for the scale-up of each reactor configuration.

4. Conclusions

A computational methodology for simulating the performance of different reactor configurations has herein been proposed in reactions with fast deactivation, as the case of methanol-to-olefins (MTO) process used as an example. The rigorous consideration

of the activity as a function of the reaction conditions has allowed the application of the kinetic parameters calculated from experimental data collected in a packed bed reactor to any reactor configuration.

The methodology is based on the resolution of the convection-dispersion-reaction equations for each lump involved in the reaction and for the activity. Different considerations of the convection and dispersion terms have led to each solid regime, including the particle circulation and mixing. An original model of parallel compartments has also been proposed in order to simulate the activity distribution function originated by the residence time distribution of solid in circulating fluidized bed reactors.

The strong influence of the temperature and water as co-feedstock in the MTO process has been well-predicted by the model. Severe reaction conditions have resulted in pronounced activity profiles in the packed bed reactor, which could be controlled by co-feeding water or using the fluidized bed reactor configuration. However, similar conversions and yields of olefins have been computed in both cases. In reactors with catalyst circulation, the simulations have predicted a short initial transitory period, subsequently reaching a steady state of activity and conversion. Moving bed reactor with counter-current direction of the gas and solid flows has offered the highest conversions for short residence times, as the fresh catalyst is always fed in the reactor zone with lower methanol concentration and maximum one of water. On the other hand, circulating fluidized bed reactor has shown the best results at conditions of longer residence times and fast deactivation. Due to the increasing interest in reactors with catalyst circulation in processes at industrial scale or in development phase (cracking, naphtha reforming, pyrolysis or gasification), the proposed methodology is presented as a useful tool for the design of these reactor configurations.

Nomenclature

a Catalyst activity

Bo Bodenstein number

C_2, C_3, C_4, HC Ethylene, propylene, butenes and rest of hydrocarbons (C_{2-6} paraffins and BTX aromatics), respectively

C-prod Carbon- containing products (OX + C_2 + C_3 + C_4 + HC)

CFBR, MBR, NCFBR, PBR Circulating fluidized bed reactor, moving bed reactor, non-circulating fluidized bed reactor and packed bed reactor, respectively

D, D_{cat} Effective dispersion coefficient of the gas and associated with the particles movement, $m^2\ h^{-1}$

$E(\tau)$, $F(\tau)$ E curve and F cummulative curve of the residence time distribution of the catalyst, respectively

F, F_r Gas total molar flow rate and gas molar flow rate in each r compartment of a CFBR model in terms of carbon, respectively, $mol_C\ h^{-1}$

f_a Activity distribution function

k_d Deactivation kinetic constant, h^{-1}

k_j Kinetic constant of each j reaction step, $mol_C\ kg^{-1}\ h^{-1}$

K_W, K_{Wd} Adsorption constant of water for reaction and deactivation rates, respectively

L Catalytic bed length, m

W/M Water-to-methanol ratio in the feed, $mol\ mol^{-1}$

N_C (Carbon molar flow rate)/(total molar flow rate) ratio, $mol_C\ mol^{-1}$

n_l, n_r, n_s Number of lumps, parallel compartments and steps of the reaction network, respectively

P Total pressure, Pa

Pe Peclet number

OX Methanol + DME lump

q_{cat}, $q_{cat,r}$ Total solid flow rate and of each r group of particles in the same compartment in the CFBR model, respectively, $m^3\ h^{-1}$

R Universal gas constant, $J\ mol^{-1}\ K^{-1}$

r_d Catalyst deactivation rate, h^{-1}

RTD Residence time distribution of the catalyst

S, S_r Section of the reactor and of each r parallel compartment in the CFBR model, respectively, m^2

T Reactor temperature, K

t Time, h

v Linear velocity of gas, $m\ h^{-1}$

v_{cat}, $v_{cat,r}$ Linear velocity of the catalyst particles and of each r group of particles in the same compartment in the CFBR model, respectively, $m\ h^{-1}$

W Water

y_i Molar fraction of each i lump in terms of carbon units, $mol_C\ mol_C^{-1}$

y_W Molar fraction of water referred to carbon units, $mol_w\ mol_C^{-1}$

z Longitudinal position in the reactor, m

Matrices and vectors

A C and O balance coefficient matrix

$\mathbf{k_j}$ Vector of the kinetic constants of each *j* reaction step, $mol_C\ kg^{-1}\ h^{-1}$

r Vector of the reaction rates of each *j* reaction step and the deactivation rate

$\mathbf{r_i}$ Vector of the formation rates of each *i* lump

$\mathbf{r_j}$ Vector of the rates of each *j* reaction step, $mol_C\ kg^{-1}\ h^{-1}$

$\mathbf{r_L}$ Vector of the reaction rates of each *i* lump and the deactivation rate

$\mathbf{y_i}$ Vector of the molar fractions of each *i* lump in terms of carbon units

Greek symbols

ε_b Effective bed-particle porosity

ρ_b Catalytic bed density, $kg\ m^{-3}$

τ, τ_r, τ_m Residence time of the catalyst particles, of each *r* group of particles in the same compartment and mean residence time of the catalyst particles, respectively, h

υ_o Methanol flow rate at the inlet of the reactor, $m^3\ h^{-1}$

Acknowledgements

This work was carried out with the support of the Ministry of Economy and Competitiveness of the Spanish Government (MINECO) cofounded with ERDF funds (CTQ2016-77812-R and CTQ2016-79646-P) and the Basque Government (IT748-13).

T. Cordero-Lanzac also acknowledges the Spanish Ministry of Education, Culture and Sport for the award of FPU grant (FPU15/01666).

References

[1] M. Argyle, C. Bartholomew, Heterogeneous Catalyst Deactivation and Regeneration: A Review, Catalysts 5 (2015) 145–269

[2] M. Guisnet, P. Magnoux, Organic chemistry of coke formation, Appl. Catal. A Gen. 212 (2001) 83–96

[3] M. Guisnet, L. Costa, F.R. Ribeiro, Prevention of zeolite deactivation by coking, J. Mol. Catal. A Chem. 305 (2009) 69–83. doi:10.1016/j.molcata.2008.11.012.

[4] H.S. Cerqueira, G. Caeiro, L. Costa, F. Ramôa Ribeiro, Deactivation of FCC catalysts, J. Mol. Catal. A Chem. 292 (2008) 1–13

[5] P. Tian, Y. Wei, M. Ye, Z. Liu, Methanol to olefins (MTO): From fundamentals to commercialization, ACS Catal. 5 (2015) 1922–1938

[6] O. Levenspiel, Chemical reaction engineering, 3rd ed., John Wiley & Sons, New York, 1999

[7] D. Kunii, O. Levenspiel, Fluidization Engineering, 2nd ed., Butterworth-Heinemann, Boston, 1991

[8] H.S. Fogler, Elements of chemical reaction engineering, 3rd ed., Prentice-Hall, 1999

[9] S. Xu, Y. Zhi, J. Han, W. Zhang, X. Wu, T. Sun, et al., Advances in catalysis for methanol-to-olefins conversion, Adv. Catal. 61 (2017) 37–122

[10] Q. Sun, Z. Xie, J. Yu, The state-of-the-art synthetic strategies for SAPO-34 zeolite catalysts in methanol-to-olefin conversion, Nat. Sci. Rev. 5 (2018) 542–

558

[11] I. Pinilla-Herrero, U. Olsbye, C. Márquez-Álvarez, E. Sastre, Effect of framework topology of SAPO catalysts on selectivity and deactivation profile in the methanol-to-olefins reaction, J. Catal. 352 (2017) 191–207

[12] P. Losch, M. Boltz, C. Bernardon, B. Louis, A. Palčić, V. Valtchev, Impact of external surface passivation of nano-ZSM-5 zeolites in the methanol-to-olefins reaction, Appl. Catal. A Gen. 509 (2016) 30–37

[13] S. Ren, G. Liu, X. Wu, X. Chen, M. Wu, G. Zeng, et al., Enhanced MTO performance over acid treated hierarchical SAPO-34, Chin. J. Catal. 38 (2017) 123–130

[14] S. Gao, S. Xu, Y. Wei, Q. Qiao, Z. Xu, X. Wu, et al., Insight into the deactivation mode of methanol-to-olefins conversion over SAPO-34: Coke, diffusion, and acidic site accessibility, J. Catal. 367 (2018) 306–314

[15] I. Yarulina, K. De Wispelaere, S. Bailleul, J. Goetze, M. Radersma, E. Abou-Hamad, et al., Structure–performance descriptors and the role of Lewis acidity in the methanol-to-propylene process, Nat. Chem. 10 (2018) 804–812

[16] X. Li, F. Rezaei, A.A. Rownaghi, Methanol-to-olefin conversion on 3D-printed ZSM-5 monolith catalysts: Effects of metal doping, mesoporosity and acid strength, Microporous Mesoporous Mater. 276 (2019) 1–12

[17] L. Qi, J. Li, L. Wang, C. Wang, L. Xu, Z. Liu, Comparative investigation of the deactivation behaviors over HZSM-5 and HSAPO-34 catalysts during low-temperature methanol conversion, Catal. Sci. Technol. 7 (2017) 2022–2031

[18] G.F. Froment, Modeling of catalyst deactivation, Appl. Catal. A Gen. 212 (2001) 117–128

[19] D. Mier, A.G. Gayubo, A.T. Aguayo, M. Olazar, J. Bilbao, Olefin production by cofeeding methanol and n-butane: kinetic modeling considering the deactivation of HZSM-5 zeolite, AIChE J. 57 (2011) 2841–2853

[20] P. Pérez-Uriarte, A. Ateka, A.G. Gayubo, T. Cordero-Lanzac, A.T. Aguayo, J. Bilbao, Deactivation kinetics for the conversion of dimethyl ether to olefins over a HZSM-5 zeolite catalyst, Chem. Eng. J. 311 (2017) 367–377

[21] T. Cordero-Lanzac, A.T. Aguayo, A.G. Gayubo, P. Castaño, J. Bilbao, Simultaneous modeling of the kinetics for n-pentane cracking and the deactivation of a HZSM-5 based catalyst, Chem. Eng. J. 331 (2018) 818–830

[22] M. Bjørgen, S. Svelle, F. Joensen, J. Nerlov, S. Kolboe, F. Bonino, et al., Conversion of methanol to hydrocarbons over zeolite H-ZSM-5: On the origin of the olefinic species, J. Catal. 249 (2007) 195–207

[23] U. Olsbye, S. Svelle, M. Bjrgen, P. Beato, T.V.W. Janssens, F. Joensen, et al., Conversion of methanol to hydrocarbons: How zeolite cavity and pore size controls product selectivity, Angew. Chem. Int. Ed. 51 (2012) 5810–5831

[24] I.M. Dahl, S. Kolboe, On the reaction mechanism for hydrocarbon formation from methanol over SAPO-34, J. Catal. 149 (1994) 458–464.

[25] T.Y. Park, G.F. Froment, Kinetic modeling of the methanol to olefins process. 1. Model formulation, Ind. Eng. Chem. Res. 40 (2001) 4172–4186

[26] W. Wu, W. Guo, W. Xiao, M. Luo, Dominant reaction pathway for methanol conversion to propene over high silicon H-ZSM-5, Chem. Eng. Sci. 66 (2011) 4722–4732

[27] P. Kumar, J.W. Thybaut, S. Svelle, U. Olsbye, G.B. Marin, Single-event microkinetics for methanol to olefins on H-ZSM-5, Ind. Eng. Chem. Res. 52

(2013) 1491–1507

[28] W. Guo, W. Wu, M. Luo, W. Xiao, Modeling of diffusion and reaction in monolithic catalysts for the methanol-to-propylene process, Fuel Process. Technol. 108 (2013) 133–138

[29] X. Huang, H. Li, W. De Xiao, D. Chen, Insight into the side reactions in methanol-to-olefin process over HZSM-5: A kinetic study, Chem. Eng. J. 299 (2016) 263–275

[30] S.M. Alwahabi, G.F. Froment, Conceptual reactor design for the methanol-to-olefins process on SAPO-34, Ind. Eng. Chem. Res. 43 (2004) 5112–5122

[31] T.V.W. Janssens, S. Svelle, U. Olsbye, Kinetic modeling of deactivation profiles in the methanol-to-hydrocarbons (MTH) reaction: A combined autocatalytic-hydrocarbon pool approach, J. Catal. 308 (2013) 122–130

[32] X. Yuan, H. Li, M. Ye, Z. Liu, Kinetic modeling of methanol to olefins process over SAPO-34 catalyst based on the dual-cycle reaction mechanism, AIChE J. 65 (2019) 662–674

[33] A.G. Gayubo, A.T. Aguayo, A.E. Sánchez del Campo, A.M. Tarrío, J. Bilbao, Kinetic modeling of methanol transformation into olefins on a SAPO-34 catalyst, Ind. Eng. Chem. Res. 39 (2000) 292–300

[34] A.N. René Bos, P.J.J. Tromp, H.N. Akse, Conversion of Methanol to Lower Olefins. Kinetic Modeling, Reactor Simulation, and Selection, Ind. Eng. Chem. Res. 34 (1995) 3808–3816

[35] A.G. Gayubo, A.T. Aguayo, A.E. Sánchez Del Campo, P.L. Benito, J. Bilbao, The role of water on the attenuation of coke deactivation of a SAPO-34 catalyst in the transformation of methanol into olefins, Stud. Surf. Sci. Catal. 126 (1999)

129–136.

[36] A.G. Gayubo, A.T. Aguayo, A. Alonso, J. Bilbao, Kinetic modeling of the methanol-to-olefins process on a silicoaluminophosphate (SAPO-18) catalyst by considering deactivation and the formation of individual olefins, Ind. Eng. Chem. Res. 46 (2007) 1981–1989

[37] A.G. Gayubo, A.T. Aguayo, A.L. Morán, M. Olazar, J. Bilbao, Role of water in the kinetic modeling of catalyst deactivation in the MTG process, AIChE J. 48 (2002) 1561–1571

[38] L. Ying, X. Yuan, M. Ye, Y. Cheng, X. Li, Z. Liu, A seven lumped kinetic model for industrial catalyst in DMTO process, Chem. Eng. Res. Des. 100 (2015) 179–191

[39] M. Luo, Y. Fu, B. Hu, D. Wang, B. Wang, G. Mao, Water inhibits the conversion and coking of olefins on SAPO-34, Appl. Catal. A Gen. 570 (2019) 209–217

[40] J. Zhang, B. Lu, F. Chen, H. Li, M. Ye, W. Wang, Simulation of a large methanol-to-olefins fluidized bed reactor with consideration of coke distribution, Chem. Eng. Sci. 189 (2018) 212–220

[41] X. Yuan, H. Li, M. Ye, Z. Liu, Study of the coke distribution in MTO fluidized bed reactor with MP-PIC approach, Can. J. Chem. Eng. 97 (2019) 500–510

[42] H. Schulz, “Coking” of zeolites during methanol conversion: Basic reactions of the MTO-, MTP- and MTG processes, Catal. Today. 154 (2010) 183–194

[43] T. Cordero-Lanzac, A. Ateka, P. Pérez-Uriarte, P. Castaño, A.T. Aguayo, J. Bilbao, Insight into the deactivation and regeneration of HZSM-5 zeolite catalysts in the conversion of dimethyl ether to olefins, Ind. Eng. Chem. Res. 57 (2018) 13689–13702

[44] Z. Wan, G.K. Li, C. Wang, H. Yang, D. Zhang, Relating coke formation and characteristics to deactivation of ZSM-5 zeolite in methanol to gasoline conversion, Appl. Catal. A Gen. 549 (2018) 141–151

[45] Y. Zhang, M. Li, E. Xing, Y. Luo, X. Shu, Coke evolution on mesoporous ZSM-5 during methanol to propylene reaction, Catal. Commun. 119 (2019) 67–70

[46] S. Müller, Y. Liu, M. Vishnuvarthan, X. Sun, A.C. Van Veen, G.L. Haller, et al., Coke formation and deactivation pathways on H-ZSM-5 in the conversion of methanol to olefins, J. Catal. 325 (2015) 48–59

[47] R.B. Rostami, M. Ghavipour, Z. Di, Y. Wang, R.M. Behbahani, Study of coke deposition phenomena on the SAPO_34 catalyst and its effects on light olefin selectivity during the methanol to olefin reaction, RSC Adv. 5 (2015) 81965–81980

[48] C.H. Collett, J. McGregor, Things go better with coke: The beneficial role of carbonaceous deposits in heterogeneous catalysis, Catal. Sci. Technol. 6 (2016) 363–378

[49] J. Zhou, J. Zhang, Y. Zhi, J. Zhao, T. Zhang, M. Ye, et al., Partial regeneration of the spent SAPO-34 catalyst in the methanol-to-olefins process via steam gasification, Ind. Eng. Chem. Res. 57 (2018) 17338–17347

[50] P. Magnoux, H.S. Cerqueira, M. Guisnet, Evolution of coke composition during ageing under nitrogen, Appl. Catal. A Gen. 235 (2002) 93–99

[51] X. Yuan, H. Li, M. Ye, Z. Liu, Comparative study of MTO kinetics over SAPO-34 catalyst in fixed and fluidized bed reactors, Chem. Eng. J. 329 (2017) 35–44

[52] A. Izadbakhsh, F. Khorasheh, Simulation of activity loss of fixed bed catalytic reactor of MTO conversion using percolation theory, Chem. Eng. Sci. 66 (2011)

6199–6208

[53] P. Bachmann, A. Bück, E. Tsotsas, Investigation of the residence time behavior of particulate products and correlation for the Bodenstein number in horizontal fluidized beds, Powder Technol. 301 (2016) 1067–1076

[54] P. Bachmann, A. Bück, E. Tsotsas, Experimental investigation and correlation of the Bodenstein number in horizontal fluidized beds with internal baffles, Powder Technol. 308 (2017) 378–387

[55] Y. Cheng, C. Wu, J. Zhu, F. Wei, Y. Jin, Downer reactor: From fundamental study to industrial application, Powder Technol. 183 (2008) 364–384

[56] G. Peng, P. Dong, Z. Li, J. Wang, W. Lin, Eulerian simulation of gas-solid flow in a countercurrent downer, Chem. Eng. J. 230 (2013) 406–414

[57] J. Zhang, G. Xu, Scale-up of bubbling fluidized beds with continuous particle flow based on particle-residence-time distribution, Particuology 19 (2015) 155–163

[58] G. Hofer, T. Märzinger, C. Eder, F. Pröll, T. Pröll, Particle mixing in bubbling fluidized bed reactors with continuous particle exchange, Chem. Eng. Sci. 195 (2019) 585–597

[59] H.S. Weng, T.L. Chen, Population balance and residence time distribution models for well-mixed reactor and regenerator system, Chem. Eng. Sci. 35 (1980) 915–924.

[60] A.G. Gayubo, J.M. Ortega, A.T. Aguayo, J.M. Arandes, J. Bilbao, MTG fluidized bed reactor-regenerator unit with catalyst circulation: Process simulation and operation of an experimental setup, Chem. Eng. Sci. 55 (2000) 3223–3235

[61] R.D. Skeel, M. Berzins, A method for the spatial discretization of parabolic equations in one space variable, SIAM J. Sci. Stat. Comput. 11 (1990) 1–32

[62] M. Shirzad, M. Karimi, J.A.C. Silva, A.E. Rodrigues, Moving Bed Reactors, Challenges and Progress of Experimental and Theoretical Studies in a Century of Research, Ind. Eng. Chem. Res. In press. doi:10.1021/acs.iecr.9b01136.

[63] M.S. Gyngazova, A. V. Kravtsov, E.D. Ivanchina, M. V. Korolenko, N. V. Chekantsev, Reactor modeling and simulation of moving-bed catalytic reforming process, Chem. Eng. J. 176–177 (2011) 134–143

[64] S. Sahebdelfar, P.M. Bijani, M. Saeedizad, F.T. Zangeneh, K. Ganji, Modeling of adiabatic moving-bed reactor for dehydrogenation of isobutane to isobutene, Appl. Catal. A Gen. 395 (2011) 107–113

[65] K.S. Kang, C.H. Kim, K.K. Bae, W.C. Cho, S.U. Jeong, S.H. Kim, et al., Modeling a counter-current moving bed for fuel and steam reactors in the TRCL process, Int. J. Hydrogen Energy 37 (2012) 3251–3260

[66] A.T. Jarullah, N.A. Awad, I.M. Mujtaba, Optimal design and operation of an industrial fluidized catalytic cracking reactor, Fuel 206 (2017) 657–674

[67] C.I.C. Pinheiro, J.L. Fernandes, L. Domingues, A.J.S. Chambel, I. Graça, N.M.C. Oliveira, et al., Fluid catalytic cracking (FCC) process modeling, simulation, and control, Ind. Eng. Chem. Res. 51 (2012) 1–29

[68] G. Lopez, M. Artetxe, M. Amutio, J. Alvarez, J. Bilbao, M. Olazar, Recent advances in the gasification of waste plastics. A critical overview, Renew. Sustain. Energy Rev. 82 (2018) 576–596